Transactions on Energy Systems and Engineering Applications

*Article*

# Thermal conductivity determination in $Fe_{78}Si_9B_{13}$/GNP/Epoxy composites by observation of samples and use of ad-hoc software: a new approximation methodology

**Pagnola Marcelo Rubén[1,3,*], Useche Jairo[2], Faig Javier[1,4], and Martínez García Ricardo[1]**

1 Instituto de Tecnologías y Ciencias de la Ingeniería, INTECIN (UBA-CONICET), Buenos Aires, Argentina.
2 Facultad de Ingeniería, Universidad Tecnológica de Bolívar, Cartagena, Colombia.
3 Departamento de Física, Facultad de Ingeniería de la Universidad de Buenos Aires, Buenos Aires, Argentina.
4 Grupo de Materiales Avanzados, Departamento de Ingeniería Mecánica, Facultad de Ingeniería de la Universidad de Buenos Aires, Buenos Aires, Argentina.
* Correspondence: mpagnola@fi.uba.ar

*Received: 30 June 2025; Accepted: 25 September 2025; Published: 06 October 2025*

**Abstract:** This study investigated the thermal conductivity ($k$) of composites composed of $Fe_{78}Si_9B_{13}$ microparticles (weight fractions: 10%, 15%, and 25%) and graphene nanoplatelets (*GNP*) (weight fractions: 0%, 1.0%, and 1.5%) embedded in a transparent epoxy matrix. Nine cylindrical samples (7 mm diameter and 2 mm length) were prepared. Thermal conductivity was determined by measuring the thermal diffusivity using the flash technique and applying the relevant relationship between the two parameters. Because some samples contained pores, the measured diffusivity was corrected for porosity by using a novel method developed by the authors. This method allowed the estimation of the composite percentage porosity based on the Young's modulus ($E$) of the sample. This correction eliminates the influence of porosity on the calculated diffusivity value, allowing determination of the intrinsic diffusivity of the composite material. Finally, the thermal conductivity of each sample was calculated using the diffusivity values. The values of the calculated parameters were compared with those determined by other well-known and established methods, and practically the same results were obtained. These comparative calculations demonstrated the efficiency of the proposed method. The results demonstrate the effectiveness of this method in correcting the effects of porosity on the thermal conductivity measurements in the studied samples.



**How to cite this article:** Pagnola, Marcelo; Useche, Jairo; Faig, Javier; Martínez, García. Thermal conductivity determination in $Fe_{78}Si_9B_{13}$/GNP/Epoxy composites by observation of samples and use of ad-hoc software: a new approximation methodology. *Transactions on Energy Systems and Engineering Applications*, 6(2): 902, 2025. DOI:10.32397/tesea.vol6.n2.902

## 1. Introduction

Materials for the manufacture of electrical transformer cores showed a significant change in their performance when soft magnetic alloys of the *FeSiB* family produced by the melt spinning technique appeared [1–4]. This technique was extended to hard magnetic alloys of the *NdFeB* family and showed versatility in the formation of cooled metallic alloys outside the equilibrium state [5]. The need to obtain cores with various designs and morphologies for the manufacture of motors, actuators, sensors, and other devices has led to the incorporation of low-energy mechanical grinding processes to obtain materials with micrometer-sized particles with or without long-range nanocrystalline ordering [6, 7]. Thus, a new family of materials with applications in electric power has emerged for the powder metallurgy industry [8]. In many cases, these are integrated with polymers to obtain materials with minimum performance requirements that are sufficient to achieve products that adequately fulfill some magnetic function. This is the case for magnetic cores manufactured in industries with high product turnover, which do not require significant energy savings during their useful life (*e.g., the toy industry*). These cores, based on powder metallurgical products, can be obtained by combining micrometer-sized magnetic particles with different polymers and/or ceramics that provide an adequate constructive design [9–11]. An advantage of this type of manufacturing is that it allows an ecological approach to Closed-Loop Production in which the original magnetic particles are recovered for subsequent recycling with a lower associated environmental impact [12–14]. Furthermore, in addition to obtaining powder metallurgical products that are sensitive to magnetic fields, materials can also be obtained that are sensitive to electric fields, and a combination of both. For this purpose, graphene and/or its oxides are added to form composites for new applications [15–17]. This is the case for the type of composite studied in this work, which is a composite material made of epoxy, graphene oxide, and *FeSiB* micrometric particle powder ($Fe_{78}Si_9B_{13}$/Graphene Nanoplatelets (GNP)/Epoxy). In this composite, each component contributes to specific properties that, when combined, define the properties of the material. In addition to the magnetic properties of the *FeSiB* particles, the combination of epoxy with graphene oxide nanoplatelets can improve the integrity of the composite, increase the cross-linking density, and optimize the mechanical and thermal conductivity properties [18, 19], and sensitivity to electric field. This is because different graphene morphologies (Graphene Oxide (GO) [20], Reduced Graphene Oxide (rGO) [21], Graphene Nanosheets [22], Graphene Platelets [23], and GNP [24]) are sensitive to the application of external electric fields. Thus, materials of this nature exhibit excellent current and heat-conducting properties [25–28]. In addition to these properties, there are other interesting ones to study, like the behavior of the properties as a function of frequency and temperature [29]. These are not considered in the scope of this article, but should be highlighted for further studies.

On the one hand, the analytical thermal conductivity models can be used to study the thermal properties of these materials, as is the case of the composite studied in this work; however, they face criticism because of their relatively low accuracy and do not incorporate the inherent challenges in the representation of the microstructural complexity of the sample [30]. On the other hand, we know that the Flash Method is the most widely used method to measure the thermal transport properties of solids because of its wide range of validity in terms of temperature and thermal conductivity [31]. The work presented herein is related to contemporize this aspect by proposing a novel method for determining the intrinsic thermal properties of these materials. Our method is based on a correction of the Flash Method, in which the porosity of the sample is considered when performing the thermal parameter calculations. The proposed method allows the estimation of the porosity based on the decrease in the Young's modulus ($E$) of the sample concerning the composite matrix. This correction eliminates the influence of porosity on the diffusivity determinate value, allowing determination of the intrinsic diffusivity of the composite. Finally, the thermal conductivity was calculated for each sample using these diffusivity values. The different calculated parameters were compared with those calculated by other well-known and established methods,

and practically the same results were obtained. These comparative calculations demonstrated the efficiency of the proposed methodology. The present work aims to contribute to the analysis and mathematical treatment of the porosity of samples, as described in the next sections.

## 2. Methods and Materials

### *2.1. Samples preparation*

The samples were prepared in the following proportions: a sample composed entirely of $Fe_{78}Si_9B_{13}$ magnetic particles after mechanical grinding, a sample formed by a mixture of $Fe_{78}Si_9B_{13}$ magnetic particles after mechanical grinding with 1% by weight of graphene nanoplates, and a sample formed by a mixture of $Fe_{78}Si_9B_{13}$ magnetic particles after mechanical grinding with 1.5% by weight of graphene nanoplates. All graphene nanoplatelets (GNP) used were obtained according to Pagnola M., Useche J. et al. [32], and the *FeSiB* powders were treated according to M. Pagnola, J. Useche, and R. Martínez García [33]. Each of the obtained mixtures was then placed in the grinding equipment, inside different containers without balls for approximately 45 min, and under low-frequency conditions (lower than those used in mechanical grinding). In this way, the samples are homogenized using little mechanical energy in the process, so as not to incorporate structural defects in the samples. The obtained powders were manually mixed in 10%, 15%, and 25% by weight proportions with two-component epoxy material (Similar to *D.E.R.* ® *331 EPOXY RESIN*). Large cylindrical specimens were obtained for each mixture, from which another smaller specimen with perfectly parallel faces was cut, as listed in Table 1.

**Table 1.** Nomenclature of obtained samples. The identical dimensions of each cylindrical sample are $7\times2$ mm.

| Composite nomenclature | Composition |
|---|---|
| 0-10 | (10 Wt% $Fe_{78}Si_9B_{13}$) in epoxy |
| 0-15 | (15 Wt% $Fe_{78}Si_9B_{13}$) in epoxy |
| 0-25 | (25 Wt% $Fe_{78}Si_9B_{13}$) in epoxy |
| 1-10 | (1 Wt% GNP + 10 Wt% $Fe_{78}Si_9B_{13}$) in epoxy |
| 1-15 | (1 Wt% GNP + 15 Wt% $Fe_{78}Si_9B_{13}$) in epoxy |
| 1-25 | (1 Wt% GNP + 25 Wt% $Fe_{78}Si_9B_{13}$) in epoxy |
| 1.5-10 | (1.5 Wt% GNP + 10 Wt% $Fe_{78}Si_9B_{13}$) in epoxy |
| 1.5-15 | (1.5 Wt% GNP + 15 Wt% $Fe_{78}Si_9B_{13}$) in epoxy |
| 1.5-25 | (1.5 Wt% GNP + 25 Wt% $Fe_{78}Si_9B_{13}$) in epoxy |

The samples described in Table 1 were used for the determination of the thermal diffusivity in Section 2.2. The samples' mechanical behavior and causes of significant changes in the properties of polymer composites with the graphene addition were discussed by Pagnola et al[32]. As said in previous paragraphs, the present work aims to only contribute to the analysis and mathematical treatment of the porosity of samples, more specifically described in Section 2.3.

### *2.2. Measurement of sample thermal diffusivity*

To measure thermal diffusivity, a system based on the flash method [34] was developed (Figure 1). In this technique, a high-intensity light and short-duration pulse is absorbed on the front surface of a thermally insulated sample a few millimeters thick. The thermal diffusivity was determined by the shape of the temperature versus time curve obtained on the back surface of the sample. In this way, with a laser pulse of aperture in the order of the measured sample (about 10 mm) the problem of thermal contact resistance is

eliminated, whereas heat losses are minimized if measurements are made in a very short time (Figure 2) and the distance from the thermistor to the outer surface of the sample is zero, as it is in contact with the sample. Therefore, in this study, we used a laser coupled to 808 nm fiber optics (*Axcel Photonics HF-808-010W-25C*) in 100 ms duration pulse emission mode with energy of 1 J, powered by a current source (*Wavelength Electronics MPL-5000*) as a pump beam to recreate the adiabatic conditions of the measurement.

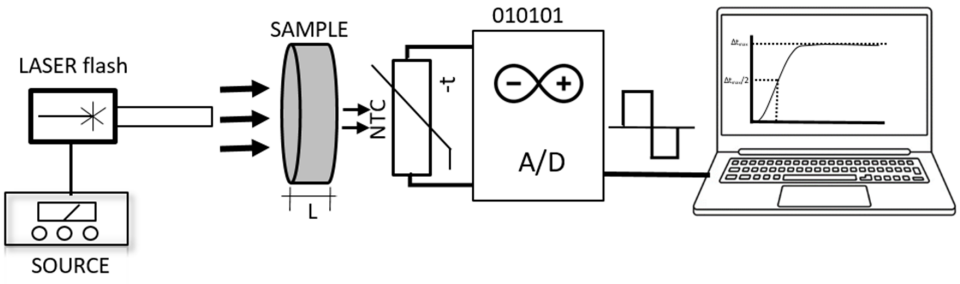


**Figure 1.** Temperature acquisition scheme by Flash method.

The temperature determination on the surface opposite to that of the incidence of the beam was carried out using a circuit equipped with operational amplifiers that follow the variation of a negative temperature coefficient thermistor, 100kΩ (NTC), and the temperature evolution variation signal was acquired using the 12-bit digital-analog converter of an Arduino UNO connected to a PC that stores the data through a program developed on the *LabView*® platform. The experiment was conducted at room temperature and the surfaces in contact were not blackened.

From the acquired data, the thermal diffusivity $D$ results [31, 35] were as follows:

$$D = \frac{0.1388 \cdot L^2}{t^*} \tag{1}$$

where $t^*$ is the time at which the amplitude of the temperature variation signal increases to half of the maximum value, and $L$ corresponds to the thickness of the sample.

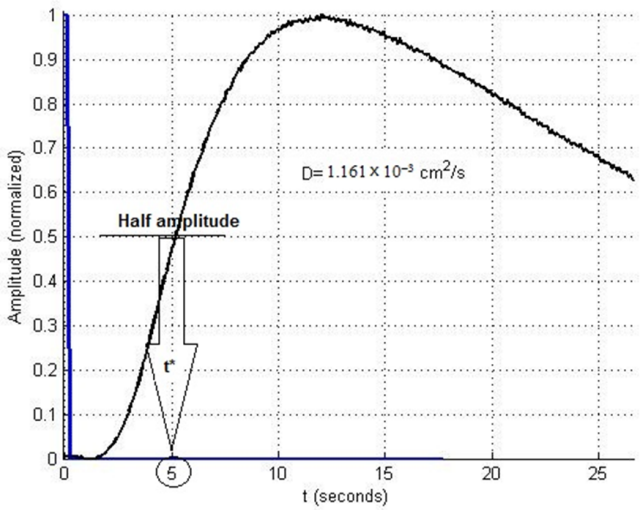


**Figure 2.** Volumetric diffusivity curve for sample 0-15.

However, if the sample has porosity, convection may occur through the pores owing to the temperature gradient, especially for large pore sizes [36]. Therefore, this diffusivity value is considered to be an effective diffusivity value ($De$) for that type of porous sample. Some samples analyzed in this work correspond to this porous type of material, as discussed in Section 2.3. The average $De$ values of three measurements on each sample for all samples are reported in Table 2.

**Table 2.** Registered values of effective diffusivity. "$X$": Sample discarded due to breakage.

| **Sample** | $De$ **[cm$^2$/s]** |
|---|---|
| 0-10 | $1.801 \times 10^{-3} \pm 7.2 \times 10^{-5}$ |
| 0-15 | $1.161 \times 10^{-3} \pm 5.8 \times 10^{-5}$ |
| 0-25 | $X$ |
| 1-10 | $1.088 \times 10^{-3} \pm 6.5 \times 10^{-5}$ |
| 1-15 | $0.994 \times 10^{-3} \pm 5.0 \times 10^{-5}$ |
| 1-25 | $0.775 \times 10^{-3} \pm 2.3 \times 10^{-5}$ |
| 1.5-10 | $0.763 \times 10^{-3} \pm 4.6 \times 10^{-5}$ |
| 1.5-15 | $0.446 \times 10^{-3} \pm 2.2 \times 10^{-5}$ |
| 1.5-25 | $0.570 \times 10^{-3} \pm 2.3 \times 10^{-5}$ |

### *2.3. Analysis of the samples porosity*

Optical microscopy analysis revealed that three of the samples studied were porous (Table 3). For these samples, the average pore size was similar (15 $\mu$m), which is explained by the fact that the methodology for obtaining these composites was the same, that is, a mechanical mixture of the components. As an example, as shown in Figure 3 shows the microstructure of the composites "sample 0-10" and "sample 0-15". A homogeneous distribution of air gas bubbles (pores) was observed in the mixture of the epoxy and metal particles. The average size of these $Fe_{78}Si_9B_{13}$ microparticles is 30 $\mu$m, which coincides with the value determined for similar microparticles obtained in previous studies [32].

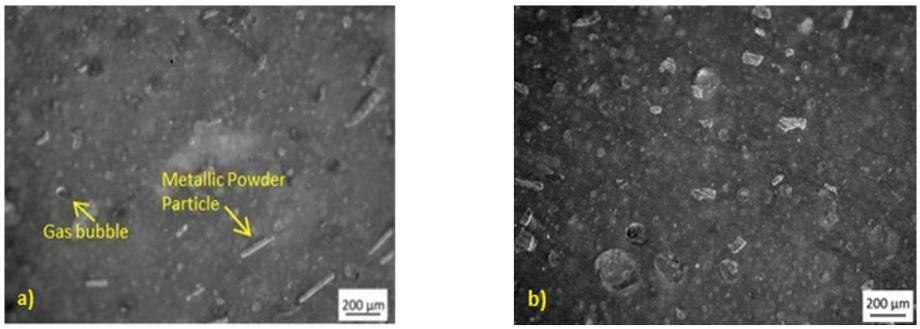


**Figure 3.** Optical micrographs of $Fe_{78}Si_9B_{13}$ powder material embedded in epoxy. a) Sample 0-10 and b) Sample 0-15.

Considering the determined average sizes, we can assume that the pores are of the same order of magnitude as metal particles. Therefore, the effect of air gas bubbles (pores) on the properties of the composites is important. To quantify this effect, it was necessary to determine the intrinsic porosity of the samples ($\varnothing$). Thus, it is possible to operate individually for each diffusivity value, as reported in Table 2. From this, the diffusivity of the solid ($D_s$) can be calculated by eliminating the effects of porosity on each sample that requires it. To calculate the intrinsic porosity, the relation observed by Rosas Yescas I. et al. [37] was used, which expresses the direct dependence of the term $(1 - \varnothing)$ on the diffusivity of the solid:

$$D_e = D_s \cdot (1 - \varnothing) \tag{2}$$

This relationship is valid up to porosity values close to 35%.

To determine the value of $D_s$ in Equation (2), it is necessary to determine the porosity values in each sample. To do so, we used the methodology and software developed by Useche J. and Pagnola M. for Functionally Graded Materials (*FGM*) [38, 39], which considers a composite of particles embedded in a matrix according to Figure 4.

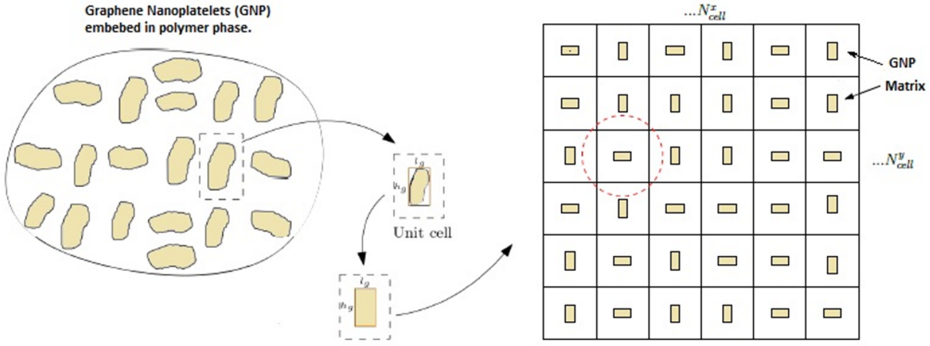


**Figure 4.** Scheme of volume representative element for the composite considered in the model developed for Nanoplatelets imbedded in matrix phase [38].

In the case of our porous material then it is necessary to run the original program by modifying the Young's modulus considered for the matrix ($E_m$). Namely, the value associated with the epoxy matrix is 0.675 GPa [27] (Figure 5). In addition to considering the effect on the graphene nanoplatelets in the programming unit cell, we must also consider the effect of the pores. Porosity has a substantial effect on mechanical properties, specifically on the mechanical resistance to bending, Young's modulus, and fracture energy [40].

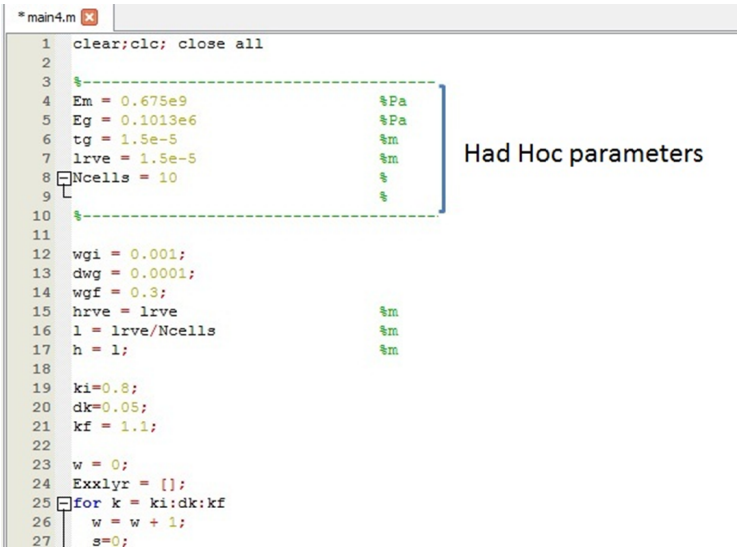


**Figure 5.** Ad Hoc parameters introduced for porous samples using the *main4.m* program [39].

To determine the percentage of porosity in the samples using the ad-hoc methodology with the software we developed [38, 39], the following elements must be considered:

1. The graphene elasticity modulus "$E_g$" is replaced by the isothermal compression modulus of air under normal pressure and temperature conditions ($E_a = 0.1013$ MPa [41]) – (See `main4.m` program in line 5 in Figure 5).
2. The characteristic pore size value (15 $\mu$m) is entered as "$tg$" and "$lrve$" values (See `main4.m` program in line 6 and line 7, over Figure 5). This establishes that the shape ratio $Lg/hg = 1$ is representative of our shape pore in study (only relationship that interests us about the set of curves obtained by executing the `main4.m` program – see Figure 6). In our case, the pore was represented as a sphere, which is compatible with what was observed by microscopy (see Figure 3a).
3. With these ad-hoc parameters entered, we run the `main4.m` program and graphically establish the desired porosity results (in abscissa), matching (in ordinate) the previously determined value of the elasticity modulus of each porous sample [32] – (see Table 3).
4. In the graph corresponding to the original software [39], the abscissa expresses the values of "Graphene Weight - $W_g$"; however, when applying i and ii points by the proposed method, the abscissa should be read as "% Porosity" – (see Figure 6).

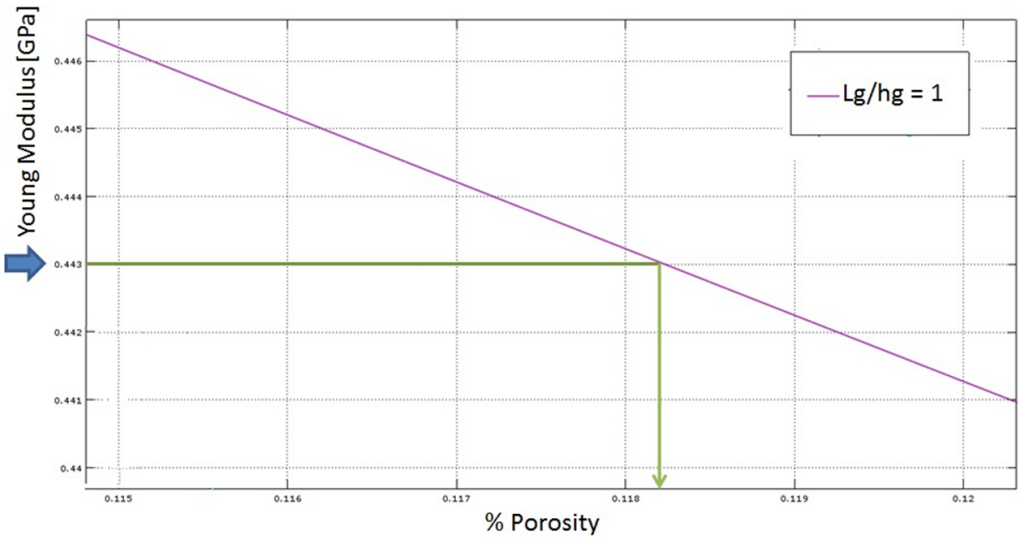


**Figure 6.** Determination of the percentage of porosity for sample 0-10 using the proposed method.

In summary, the main objective of this method is to determine the percentage of porosity in the sample by incorporating the ad-hoc parameters "air elasticity modulus" and "pore shape ratio" into the calculation of the elasticity modulus on a previously designed program for Functionally Graded Materials (*FGM*). By introducing these parameters, the aim is to adjust experimental elasticity modulus value (see the second column in Table 3) with the obtained main adjustment variable is the percentage of porosity. By graphic adjusting of elasticity modulus in ordinate (experimental value observed in [32]) the percentage of porosity in the composite was obtained in abscissa in Figure 6. In Table 3 are listed all the values.

**Table 3.** Experimental elasticity modulus values [32] and porosity percentage values corresponding to the studied samples.

| Sample | $E$ [GPa] | % Porosity |
|---|---|---|
| 0-10 | 0.4432 | 11.82 |
| 0-15 | 0.6995 | Not observed |
| 1-10 | 0.2857 | 33.71 |
| 1-15 | 0.6790 | Not observed |
| 1-25 | 0.8110 | Not observed |
| 1.5-10 | 0.8906 | Not observed |
| 1.5-15 | 0.8745 | Not observed |
| 1.5-25 | 0.5416 | 3.62 |

## 3. Results

### *3.1. Solid diffusivity value ($D_s$)*

Using the percentage porosity values determined in Section 2.3, we can determine the solid diffusivity values ($D_s$) using Equation (2). The values are presented in Table 4.

**Table 4.** Effective diffusivity ($D_e$) and corrected diffusivity ($D_s$) values corresponding to the studied samples. Values that were corrected using the proposed methodology (composites with porous matrix) are indicated in green.

| Sample | $D_e$ [cm$^2$/s] | $D_s$ [cm$^2$/s] |
|---|---|---|
| 0-10 | $1.801 \times 10^{-3} \pm 7.2 \times 10^{-5}$ | $2.043 \times 10^{-3} \pm 1.0 \times 10^{-4}$ |
| 0-15 | $1.161 \times 10^{-3} \pm 5.8 \times 10^{-5}$ | $1.161 \times 10^{-3} \pm 5.8 \times 10^{-5}$ |
| 1-10 | $1.088 \times 10^{-3} \pm 6.5 \times 10^{-5}$ | $1.641 \times 10^{-3} \pm 1.1 \times 10^{-4}$ |
| 1-15 | $0.994 \times 10^{-3} \pm 5.0 \times 10^{-5}$ | $0.994 \times 10^{-3} \pm 5.0 \times 10^{-5}$ |
| 1-25 | $0.775 \times 10^{-3} \pm 2.3 \times 10^{-5}$ | $0.775 \times 10^{-3} \pm 2.3 \times 10^{-5}$ |
| 1.5-10 | $0.763 \times 10^{-3} \pm 4.6 \times 10^{-5}$ | $0.763 \times 10^{-3} \pm 4.6 \times 10^{-5}$ |
| 1.5-15 | $0.446 \times 10^{-3} \pm 2.2 \times 10^{-5}$ | $0.446 \times 10^{-3} \pm 2.2 \times 10^{-5}$ |
| 1.5-25 | $0.570 \times 10^{-3} \pm 2.3 \times 10^{-5}$ | $0.591 \times 10^{-3} \pm 3.5 \times 10^{-5}$ |

Substituting the values of $D_s$ (Table 4) into Equation (3), we can obtain the thermal conductivity values for the studied composites ($k_{\text{comp}}$). The density of the solid ($\rho_{\text{comp}}$) that must be considered in Equation (3) is that of the composite material. The specific heat ($c_{p\,\text{comp}}$) used in this expression is the result of the specific heat of each sample component. To calculate the values associated with the composites, Equations (4) and (5) and the data contained in Table 5 must be used.

$$D_s = \frac{k_{\text{comp}}}{\rho_{\text{comp}} \cdot c_{p\,\text{comp}}} \tag{3}$$

where:

- $k_{\text{comp}}$: Thermal conductivity of composite [W/mK]
- $\rho_{\text{comp}}$: Solid density of composite [kg/m$^3$]
- $c_{p\,\text{comp}}$: Specific heat of the composite at constant pressure [J/kgK]
- $D_s$: Solid thermal diffusivity [m$^2$/s]

**Table 5.** Values used in Equations (4) and (5) to calculate the thermal conductivity of the composites $k_{\text{comp}}$.

| **Material** | $\rho$ [kg/m$^3$] | $c_p$ [J/kgK] | $k$ [W/mK] | **References** |
|---|---|---|---|---|
| $Fe_{78}Si_9B_{13}$ | 7500 | 484 | 79.41 | [42] |
| GNP | 260 | 1400 | 0.43 | [43] |
| Epoxy | 1160 | 1940 | 0.196 | [44–46] |

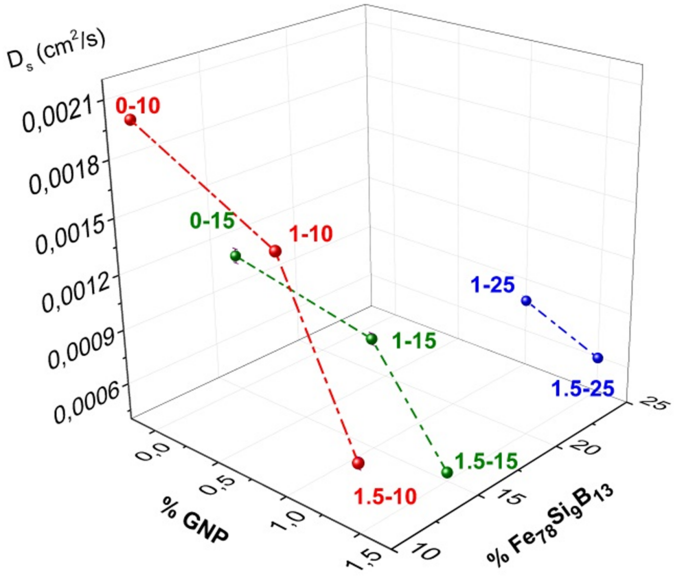


**Figure 7.** $D_s$ trends with the concentrations of components in the composites. **Note:** $D_{\text{epox}} = 8.419 \times 10^{-3}\,\text{cm}^2/\text{s}$ (Value obtained according to Table 5 and [45,46]).

The composite density ($\rho_{\text{comp}}$) and composite specific heat ($C_{p\,\text{comp}}$) values were determined using Equations (4) and (5). These values were substituted into Equation (3), and the obtained results ($k_{\text{comp}}$) are listed in Table 6.

$$\rho_{\text{comp}} = \%V_{(\text{FeSiB})} \cdot \rho_{(\text{FeSiB})} + \%V_{(\text{GNP})} \cdot \rho_{(\text{GNP})} + \%V_{(\text{Epx})} \cdot \rho_{(\text{Epx})} \tag{4}$$

$$C_{p\,\text{comp}} = \%W_{t,(\text{FeSiB})} \cdot C_{p(\text{FeSiB})} + \%W_{t(\text{GNP})} \cdot C_{p(\text{GNP})} + \%W_{t(\text{Epx})} \cdot C_{p(\text{Epx})} \tag{5}$$

### *3.2. Thermal conductivity determination*

To obtain the thermal conductivity of each composite ($k_{\text{comp}}$ values reported in Table 6), the Flash Method contained in Equation (3) and explained in Section 3.1, was used because this method is one of the most commonly used methods to determine the $k$ values in composite materials with a polymer matrix. It is a nonstationary method with reliable results when measurements made on small samples are used (as is the case in this work). With nonstationary methods, a wide range of thermal conductivities can be measured in most polymers and polymeric composites. Thermal diffusivity measurement using the laser flash method is the most commonly used method for these cases [47].

**Table 6.** Thermal conductivity values corresponding to the studied samples ($k_{\text{comp}}$).

| Sample | $\rho_{\text{comp}}$ [kg/m$^3$] | $c_{p\,\text{comp}}$ [J/kgK] | $k_{\text{comp}}$ [W/mK] |
|---|---|---|---|
| 0-10 | $1000.8 \pm 20.02$ | $1794.4 \pm 35.89$ | $0.3671 \pm 3.30 \times 10^{-2}$ |
| 0-15 | $1327.7 \pm 26.55$ | $1721.7 \pm 34.43$ | $0.2654 \pm 2.40 \times 10^{-2}$ |
| 0-25 | $x$ | $x$ | $x$ |
| 1-10 | $932.1 \pm 19.01$ | $1779.3 \pm 35.60$ | $0.2722 \pm 2.70 \times 10^{-2}$ |
| 1-15 | $1277.8 \pm 28.14$ | $1707.4 \pm 34.20$ | $0.2169 \pm 2.00 \times 10^{-2}$ |
| 1-25 | $1406.9 \pm 23.98$ | $1563.5 \pm 31.27$ | $0.1705 \pm 1.20 \times 10^{-2}$ |
| 1.5-10 | $1199 \pm 28.14$ | $1771.8 \pm 35.45$ | $1.6209 \pm 1.60 \times 10^{-1}$ |
| 1.5-15 | $1253.7 \pm 25.07$ | $1700.2 \pm 34.00$ | $0.9507 \pm 8.56 \times 10^{-2}$ |
| 1.5-25 | $1380 \pm 27.60$ | $1557.2 \pm 31.15$ | $0.1271 \pm 1.27 \times 10^{-2}$ |

**Note:** "$x$" means sample not considered.

Figure 8 shows the thermal conductivities of the composites. A trend of the $k_{comp}$ value as a function of the sample composition was observed.

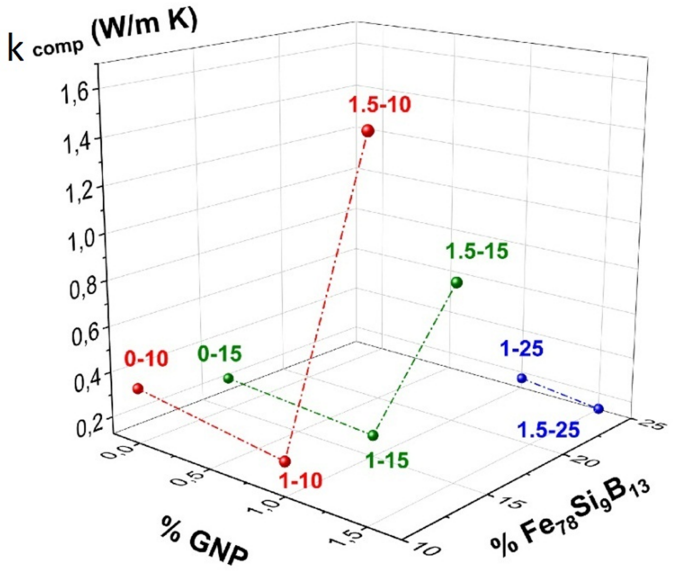


**Figure 8.** $k_{comp}$ value as a function of the sample composition.

## 4. Discussion

Composite properties are a combination of the properties of each material that composes it. In this study, samples were obtained from materials with various electronic structures that determine a general behavior different from their individual physical properties. The insulating matrix is formed by a polymer composed of chains of light atoms with relatively weak atomic bonds. They are distributed in the matrix magnetic microparticles of $Fe_{78}Si_9B_{13}$ and graphene nanoplatelets (GNP) appear. These materials exhibited different thermal conductivities. $Fe_{78}Si_9B_{13}$ is a mostly amorphous material, which favors ionic conductivity owing to its disordered structure and constitutes strong atomic bonds with metallic properties of ductility and malleability that are quite different from those of graphene. Furthermore, for some of the composites studied in this work, the disturbance in the properties caused by the polymer matrix porosity must be

considered. In this regard, it must be considered that in these samples, the average pore size is on the order of the size of the $Fe_{78}Si_9B_{13}$ particles (see Figure 3 and the associated analysis in Section 2.3). It is known that pores in most cases are neither spherical nor cylindrical, but are a series of tortuous paths, with interconnections consisting of paths with variable section areas, so the effective diffusivity in samples of this type can be considered with Equation (6):

$$D_e = D_s \cdot \frac{\varnothing}{\tau} \tag{6}$$

where $\phi$ is the porosity and $\tau$ is the tortuosity, which depends on the cavernous structure of the porous sample. The $\phi/\tau$ ratio can have values ranging from 0.219 for artificial granules to 0.55 for branched granules [48]. When the pore structure is formed by an intricate interconnection of pores, the effect on the decrease in the diffusivity of the solid is much greater than if the structure is formed by practically isolated spherical pores. The latter case best fits the porous samples studied in this work (see Figure 3). Therefore, the use of Equation (2) was justified in our analysis. Although some authors consider that the effective diffusivity increases with porosity, there is another criterion: for porosity percentages on the order of 30% or less, the molecules experience a greater degree of geometric confinement, and the pore walls limit their movement, with a progressive decrease in diffusivity [49]. That is, there is a percolation threshold, which for an infinite network, such as that used the development software [39], is close to 0.313 [49]. This percolation threshold is consistent with the model proposed in the methodology proposed in this study [37].

It can be assumed that the highest values of diffusivity and thermal conductivity will be obtained for the composites in which the $Fe_{78}Si_9B_{13}$ particles are closer to each other, a situation that would be the most favorable for the metallic ions that compose them to interact with each other and maximize the conduction properties of the composite in the presence of thermal flow. The maximum proximity between the $Fe_{78}Si_9B_{13}$ particles occurred when the composite was formed only by these particles distributed in an epoxy matrix that did not exhibit porosity. The experiment confirmed that increasing the concentration of GNP caused a decrease in the thermal diffusivity ($D_s$). The incorporation of graphene nanoplatelets caused an increase in the distance between the metal ions, which in turn determined the magnitude of $D_s$ in the sample volume. To higher the amount of GNP in the composite, weaker is the interaction between the $Fe_{78}Si_9B_{13}$ particles, and the lower the $D_s$ value. Figures 7 and 8 show that this trend is the same regardless of the percentage of $Fe_{78}Si_9B_{13}$ particles that make up the composite (10%, 15%, or 25% $Fe_{78}Si_9B_{13}$ series).

However, an opposite effect on the thermal conductivity ($k_{\text{comp}}$) was observed; this magnitude increased as the amount of GNP in the sample increased. This is associated with the different electronic natures of GNP and $Fe_{78}Si_9B_{13}$, which is manifested in that the GNP heat capacity is up to 65% higher than that of $Fe_{78}Si_9B_{13}$ particles (see Table 5). Such a difference in the heat capacity values leads to an increase in the thermal conductivity of the composite as the amount of GNP increases. It appears that the effect of incorporating GNP is to channel the excitation caused by the thermal flow and increase the capacity of the composite to transmit heat. It is known that for amorphous or semi-crystalline polymers, including epoxies, the heat conduction is very low because phonon scattering occurs mainly in the amorphous phase [50]. However, the incorporation of GNP into the matrix creates a more effective path for phonon conduction, thereby increasing the thermal conductivity [19].

It should be noted that in the previous analysis, materials with no porosity were compared, because this has been corrected with the methodology explained in this manuscript. If the effect of porosity is analyzed, the pores would also have to be considered as distancing agents of the $Fe_{78}Si_9B_{13}$ particles, which would affect the interaction between them and would contribute a priori to impacting the diffusivity values. This is what happens with this type of sample, and modifies the properties discussed in this article. Therefore,

applying the methodology developed in this study allowed us to correct the behavior of the samples for porosity (see Figure 6 and Table 4). In this sense, our methodology is validated by first comparing the porosity and thermal conductivity values with the results obtained by other authors. In this way, the porosity results obtained with our methodology reported in Table 3 are validated with the Luping model [51], which considers the elastic modulus of a composite ($E^*$) to be directly proportional to the effective area fraction or the area of the matrix ($A_m$) according to Equations (7) and (8):

$$E^* = E_m \cdot A_m \tag{7}$$

$$A_m = 1 - kd \cdot \phi^{2/3} \tag{8}$$

Where: $kd = 1.21$ (spherical pore) [40].

Our experimental determination of elasticity modules, reported in Section 2.3 determines a maximum average error of 4% comparative in form with the other models considered. This allows us to ensure that the decrease in the elasticity modulus found experimentally in the samples refers to the porous effect proposed by our methodology, and that the porosity values are consistent (see Table 7).

**Table 7.** Comparison between elasticity modulus of experimental samples with porosity ($E$) and Luping model elasticity modulus ($E^*$).

| **Sample** | $E$ **[GPa]** | **% Porosity** | $A_m$ | $E^*$ **[GPa]** |
|---|---|---|---|---|
| 0-10 | 0.4432 | 11.82 | 0.7089 | 0.4783 |
| 1-10 | 0.2857 | 33.71 | 0.4140 | 0.2794 |
| 1.5-25 | 0.5416 | 3.62 | 0.8680 | 0.5856 |

This wide range of porosities covered by the proposal is discussed by applying models that study finite particles and/or gas-filled void spaces embedded in a continuous medium [50, 52] as follows:

- Maxwell Theoretical Model (MTM), which considers the conductivity of randomly distributed homogeneous spheres that do not interact in a homogeneous continuous medium.
- Series Model (SM), where the continuous medium interacts directly with the discrete phase.
- Geometric Mean Model (GMM), where the discrete phase interacts nonlinearly with the continuous phase.
- The Nielsen Model (NM), which has a relatively simple formulation and is applied to a wide range of composite materials [53].

To compare the obtained values for the thermal conductivity in the composite using the methodology presented in this work, the values of the mentioned models should be considered.

**Serie Model (SM)**

$$k_e = (1 - V_{df})\, k_c + V_{df}\, k_d \tag{9}$$

**Geometric Mean Model (GMM)**

$$k_e = k_d^{V_{df}}\, k_c^{(1-V_{df})} \tag{10}$$

**Maxwell Theoretical Model (MTM)**

$$k_e = k_c \cdot \left[ \frac{(k_d + 2k_c + 2V_{df}(k_d - k_c))}{(k_d + 2k_c - V_{df}(k_d - k_c))} \right] \tag{11}$$

**Nielsen Model (NM)**

$$k_e = k_c \cdot \left[\frac{1 + A\,B\,V_{df}}{1 - B\,\beta\,V_{df}}\right] \tag{12}$$

where: $A$: adimensional shape factor which depends on the geometry of the particles (spheres randomly) [52, 53].

$$B = \frac{k_d/(k_c - 1)}{k_d/(k_c + A)} \tag{12.1}$$

$$\beta = 1 + \left[\frac{(1 - V_m)}{V_m^2}\right] \cdot V_{df} \tag{12.2}$$

$$V_m = 0.6 \quad \text{(spheres)} \tag{12.3}$$

where:

- $k_e$: Thermal conductivity of the composite.
- $V_{df}$: Volume fraction of the discrete phase.
- $k_c$: Thermal conductivity of the continuous phase.
- $k_d$: Thermal conductivity of the discrete phase.

For the application of these models, we used the values of thermal conductivity of the continuous phase ($k_c$) obtained in Table 6, the value of $k_d$ is the thermal conductivity of the air (0.024 W/m·K [54]), and the volume fraction of the discrete phase ($V_{df}$) was utilized as the porosity values reported in Table 3. Table 8 was obtained using these values.

**Table 8.** Values of thermal conductivity for composite samples obtained by applying Equations (6) to (9). "x": sample not considered.

| **Sample** | $k_c$ [W/m·K] | $k_e$ [W/m·K] | | | | |
|---|---|---|---|---|---|---|
| | | *Experimental* | *SM* | *GMM* | *MTM* | *NM* |
| 0-10 | 0.3671 | 0.3234 | 0.3263 | 0.2654 | 0.3108 | 0.3134 |
| 0-15 | 0.2654 | 0.2654 | 0.2654 | 0.2654 | 0.2654 | 0.2654 |
| 0-25 | x | x | x | x | x | x |
| 1-10 | 0.2722 | 0.1804 | 0.1895 | 0.1201 | 0.1674 | 0.1667 |
| 1-15 | 0.2169 | 0.2169 | 0.2169 | 0.2169 | 0.2169 | 0.2169 |
| 1-25 | 0.1705 | 0.1705 | 0.1705 | 0.1705 | 0.1705 | 0.1705 |
| 1.5-10 | 1.6209 | 1.6209 | 1.6209 | 1.6209 | 1.6209 | 1.6209 |
| 1.5-15 | 0.9507 | 0.9507 | 0.9507 | 0.9507 | 0.9507 | 0.9507 |
| 1.5-25 | 0.1271 | 0.1225 | 0.1234 | 0.1197 | 0.1220 | 0.1223 |

**Note:** The experimental values are directly linked to the effective diffusivity ($D_e$) of the porous solid reported in Table 2.

In Table 8 it can be observed that the thermal conductivity of the composite (porous case) is described in a very similar way to any of the models discussed. These values correspond in such a way that most of the models referring to the same continuous solid can be used, except for the Geometric Mean Model (which shows a difference of 33% with respect to the experimental values). On the other hand, the rest of the models fit error values between 4.5 – 8 % for the case of higher porosity found in sample 1-10. These cases cover various approximations that are necessary to validate the proposed methodology.

However, must be remembered that in anisotropic materials (this is the case of the composites studied), the thermal conductivity varies with the orientation and is expressed exactly by a second-order tensor [19, 55]. Therefore, the methodology treated in this work is an approximate determination method, as is the case with the models with which it was compared.

## 5. Conclusions

This paper discusses a new approximation methodology that allows the estimation of the percentage of porosity in $Fe_{78}Si_9B_{13}$/*GNP*/Epoxy composites using software designed to treat the mechanical behavior of Functionally Graded Materials (*FGM*). With this method, it is possible to additionally correct the determination of the composite diffusivity values by eliminating the effect of found porosity. The effect of porosity is associated with thermal gradient changes inside the pores, and the determination of the thermal magnitudes is distorted. These corrections allow the composite conductivity value to be obtained from the value determined for the solid diffusivity using the relationship reported in Equation (2). This expression allows determination of the conductivity for samples with a high percentage of porosity (case of composite 1-10 that has 33.7% porosity, see Table 3). Using the calculation treatment explained in the present work, we were able to determine conductivity values of the samples that only differed between 1% and 8% from the values calculated by other models with which we compared. This comparison validated the model proposed and reported in this study. In this regard, we verified that by eliminating the porosity effects in the samples, the thermal conductivity increased with the addition of *GNP* to the composite. The addition of *GNP* also affected the diffusivity of the samples. This value decreases with increasing *GNP* content in the composite owing to the change in the resistivity and specific heat values in the sample. It was also observed that incorporating *GNP* into the composite above 1% by weight changes the thermal conductivity independent of the content of $Fe_{78}Si_9B_{13}$ particles in the sample. Finally, although this methodology is used to derive the thermal conductivity data from the thermal diffusivity data, the method proposed in this work is perfectly comparable, for porosities below the percolation threshold, with the most common models used in the literature. As shown in Table 7. The comparison above allows us to infer that the proposed methodology is adequate for the purposes pursued.

## Acknowledgments

The authors appreciate the participation of Dr. Ferrari S. and CPA CONICET worker Eng. Rodrigo Cancillieri and Mr. Camilo Abecian. We also thank Dr. Facundo Zaldivar and Dr. Luis Emiliano Jan for performing the diffusivity measurements of the samples.

**Funding:** This work was supported by the Universidad de Buenos Aires under Grant UBACyT 20020190100046BA and CONICET support funds.

**Author contributions:** M.R.P. elaborated on the fundamental idea of this work and drafted the initial manuscript, which was subsequently revised for J.U. The figures in this manuscript have been developed and reviewed by J.F, who coordinated the measurements of the samples and their preparation, together with R.M.G. The control of the information and bibliographic search has been a contribution of all the authors.

**Disclosure statement:** The authors declare no conflict of interest.

**Data availability statement:**

Any additional data or information to obtain program codes can be freely accessed at: http://hdl.handle.net/11336/235587 or write to the corresponding author.

## References


[1] T Egami. Magnetic amorphous alloys: physics and technological applications. *Reports on Progress in Physics*, 47(12):1601–1725, December 1984.

[2] Davor Pavuna. Production of metallic glass ribbons by the chill-block melt-spinning technique in stabilized laboratory conditions. *Journal of Materials Science*, 16(9):2419–2433, September 1981.

[3] Marcelo Rubén Pagnola, Jairo Useche Vivero, and Andrés G. Marrugo. *Magnetic Materials by Melt Spinning Method, Structural Characterization, and Numerical Modeling*. InTech, October 2018.

[4] M. Pagnola, M. Malmoria, and M. Barone. Biot number behaviour in the chill block melt spinning (cbms) process. *Applied Thermal Engineering*, 103:807–811, June 2016.

[5] D. Derewnicka-Krawczyńska, S. Ferrari, V. Bilovol, M. Pagnola, K. Morawiec, and F.D. Saccone. Influence of nb, mo, and ti as doping metals on structure and magnetic response in ndfeb based melt spun ribbons. *Journal of Magnetism and Magnetic Materials*, 462:83–95, September 2018.

[6] P.H. Shingu. *Mechanical Alloying*. Trans Tech Publications Ltd, January 1992.

[7] Hywel A. Davies and Michael R.J. Gibbs. Amorphous alloys, July 2007.

[8] Fabiana Morales, Marcelo Rubén Pagnola, Juan José Muriel, and Leandro Martín Socolovsky. Molienda mecánica sobre cintas magnéticas blandas de fe78si9b13 con molino de bolas ortorrómbico de fabricación propia. 2020.

[9] Fatma Ozdemir, Iain Evans, Kenneth S. Rankin, and Oana Bretcanu. Preliminary evaluation of the in vitro biocompatibility of magnetic bone cement composites. *Open Ceramics*, 7:100146, September 2021.

[10] Zhuang Tian, Yancheng Li, Jiajia Zheng, and Shuguang Wang. A state-of-the-art on self-sensing concrete: Materials, fabrication and properties. *Composites Part B: Engineering*, 177:107437, November 2019.

[11] Wenyao Li, Han Gu, Zhihao Liu, Haiwei Zhang, Li Jiang, and Xing Zhou. Research progress in the synthesis and application of magnetic self-healing polymer composites. *European Polymer Journal*, 202:112633, January 2024.

[12] Pei-Xiu Tian, Yi-Dong Li, Zhi Hu, and Jian-Bing Zeng. Fire-resistant and high-performance epoxy vitrimers for fully recyclable carbon fiber-reinforced composites. *Materials Today Chemistry*, 36:101965, March 2024.

[13] M. Ramzan, Raphael M. Obodo, Hope E. Nsude, M.I. Shahzad, Ishaq Ahmad, and Fabian Ezema. *Functionalized ceramic matrix composites: Fabrication, application, and recycling*, page 189–204. Elsevier, 2023.

[14] Ester M. Palmero, Javier Rial, Javier de Vicente, Julio Camarero, Björn Skårman, Hilmar Vidarsson, Per-Olof Larsson, and Alberto Bollero. Development of permanent magnet mnalc/polymer composites and flexible filament for bonding and 3d-printing technologies. *Science and Technology of Advanced Materials*, 19(1):465–473, May 2018.

[15] Driss Kenfaui, Zarel Valdez-Nava, Lionel Laudebat, Marie-Laure Locatelli, Céline Combettes, Vincent Bley, Sorin Dinculescu, Christophe Tenailleau, Pascal Dufour, and Sophie Guillemet-Fritsch. Innovative ceramic-matrix composite substrates with tunable electrical conductivity for high-power applications. *Science and Technology of Advanced Materials*, 23(1):735–751, November 2022.

[16] Md Habibur Rahaman, Usman Yaqoob, and Hyeon Cheol Kim. The effects of conductive nano fillers alignment on the dielectric properties of copolymer matrix. *Advanced Manufacturing: Polymer amp; Composites Science*, 5(1):29–36, January 2019.

[17] Weifeng Zhao, Ming Fang, Furong Wu, Hang Wu, Liwei Wang, and Guohua Chen. Preparation of graphene by exfoliation of graphite using wet ball milling. *Journal of Materials Chemistry*, 20(28):5817, 2010.

[18] Ming Dong, Han Zhang, Lazaros Tzounis, Giovanni Santagiuliana, Emiliano Bilotti, and Dimitrios G. Papageorgiou. Multifunctional epoxy nanocomposites reinforced by two-dimensional materials: A review. *Carbon*, 185:57–81, November 2021.

[19] Mulan Mu, Chaoying Wan, and Tony McNally. Thermal conductivity of 2d nano-structured graphitic materials and their composites with epoxy resins. *2D Materials*, 4(4):042001, August 2017.

[20] Jiadong Qin, Yubai Zhang, Sean E. Lowe, Lixue Jiang, Han Yeu Ling, Ge Shi, Porun Liu, Shanqing Zhang, Yu Lin Zhong, and Huijun Zhao. Room temperature production of graphene oxide with thermally labile oxygen functional groups for improved lithium ion battery fabrication and performance. *Journal of Materials Chemistry A*, 7(16):9646–9655, 2019.

[21] R.P. Reshma, N.S. Abishek, and K. Naik Gopalakrishna. Synthesis and characterization of graphene oxide, tin oxide, and reduced graphene oxide-tin oxide nanocomposites. *Inorganic Chemistry Communications*, 165:112451, July 2024.

[22] In-Yup Jeon, Yeon-Ran Shin, Gyung-Joo Sohn, Hyun-Jung Choi, Seo-Yoon Bae, Javeed Mahmood, Sun-Min Jung, Jeong-Min Seo, Min-Jung Kim, Dong Wook Chang, Liming Dai, and Jong-Beom Baek. Edge-carboxylated graphene nanosheets via ball milling. *Proceedings of the National Academy of Sciences*, 109(15):5588–5593, March 2012.

[23] Ge Shi, Sherif Araby, Christopher T. Gibson, Qingshi Meng, Shenmin Zhu, and Jun Ma. Graphene platelets and their polymer composites: Fabrication, structure, properties, and applications. *Advanced Functional Materials*, 28(19), March 2018.

[24] Fuan He, Kwokho Lam, Dong Ma, Jintu Fan, Laiwa Helen Chan, and Liming Zhang. Fabrication of graphene nanosheet (gns)–fe3o4 hybrids and gns–fe3o4/syndiotactic polystyrene composites with high dielectric permittivity. *Carbon*, 58:175–184, July 2013.

[25] J. Kováčik and Š. Emmer. Cross property connection between the electric and the thermal conductivities of copper graphite composites. *International Journal of Engineering Science*, 144:103130, November 2019.

[26] Hanhai Dong, Yixuan Qiao, Song Peng, Yuqi Li, Yongqian Zhen, Wei Tan, Qingli Cheng, and Yang Wang. 2d material/epoxy composite coatings, a perspective from the regulation of 2d materials. *Progress in Organic Coatings*, 183:107817, October 2023.

[27] N I C Berhanuddin, I Zaman, S A M Rozlan, M A A Karim, B Manshoor, A Khalid, S W Chan, and Q Meng. Enhancement of mechanical properties of epoxy/graphene nanocomposite. *Journal of Physics: Conference Series*, 914:012036, October 2017.

[28] Jorge Peña-Consuegra, Marcelo R. Pagnola, Jairo Useche, Pagidi Madhukar, Fabio D. Saccone, and Andrés G. Marrugo. Manufacturing and measuring techniques for graphene-silicone-based strain sensors. *JOM*, 75(3):631–645, October 2022.

[29] J. Ross Macdonald. Impedance spectroscopy. *Annals of Biomedical Engineering*, 20(3):289–305, May 1992.

[30] Dongil Shin, Peter Jefferson Creveling, Scott Alan Roberts, and Rémi Dingreville. Deep material network for thermal conductivity problems: Application to woven composites. *Computer Methods in Applied Mechanics and Engineering*, 431:117279, November 2024.

[31] Wolfgang Buck and Steffen Rudtsch. *Thermal Properties*, page 399–429. Springer Berlin Heidelberg, 2006.

[32] Marcelo Ruben Pagnola, Jairo Useche, Javier Faig, Sergio Ferrari, and Ricardo Martinez Garcia. Study of the properties of a composite material fe78si9b13 / gnp in an epoxy matrix. *Transactions on Energy Systems and Engineering Applications*, 5(1), April 2024.

[33] Marcelo Pagnola, Jairo Useche V., and Ricardo Martinez García. Obtención de fe78si9b13/gnpl composite: Un estudio de propiedades, July 2023.

[34] W. J. Parker, R. J. Jenkins, C. P. Butler, and G. L. Abbott. Flash method of determining thermal diffusivity, heat capacity, and thermal conductivity. *Journal of Applied Physics*, 32(9):1679–1684, September 1961.

[35] Bochuan Lin, Heng Ban, Chao Li, Rosalia N. Scripa, Ching-Hua Su, and Sandor L. Lehoczky. Method for obtaining thermal conductivity from modified laser flash measurement. In *Heat Transfer, Part B*, IMECE2005, page 725–730. ASMEDC, January 2005.

[36] Ismail Tavman. Flash method of measuring thermal diffusivity and conductivity. In *Convective Heat and Mass Transfer in Porous Media*, pages 923–936. Springer, 1991.

[37] Israel Rosas Yescas, José Eduardo Acosta Cano de los Ríos, Óscar Arturo Chávez López, Carlos Arturo Méndez Herrera, and Victor Manuel Ambríz Díaz. Evaluación de la difusividad térmica efectiva en el estado transitorio de una geometría fractal para condiciones de temperatura y flujo de calor constantes. *Ciencia Nicolaita*, (89), August 2023.

[38] J. Useche and M. Pagnola. Vibration analysis of functionally graded epoxy/graphene composite plates using the boundary element method and new micromechanical model. *Mechanics of Advanced Materials and Structures*, 32(5):923–933, May 2024.

[39] Marcelo Rubén Pagnola. Analytical micromechanical model. Dataset, 2024.

[40] F Sandoval and Alberto Ibáñez Rodríguez. Discusión sobre la influencia de la porosidad en la resistencia mecánica de las baldosas cerámicas. 2000.

[41] Marvin L. Cohen. Calculation of bulk moduli of diamond and zinc-blende solids. *Physical Review B*, 32(12):7988–7991, December 1985.

[42] Chunbai Wang. *Numerical modeling of free surface and rapid solidification for simulation and analysis of melt spinning*. PhD thesis, Iowa State University.

[43] HNWNanomaterial. Graphene nanosheet for high heat conduction use. https://es.hwnanomaterial.com/graphene-nanosheet-for-high-heat-conduction-use_p522.html, 2025. Accessed: 2025-10-02.

[44] Igor Novak, Ludovit Kubicar, C Anibarro, Viliam Vretenár, Peter Dieška, Ismail Tavman, and Ivan Chodák. Thermal conductivity of crosslinking epoxy resin. 06 2014.

[45] D.e.r.r 331 epoxy resin - technical datasheet. https://cstjmateriauxcomposites.wordpress.com/wp-content/uploads/2017/11/der331.pdf, 2017. Accessed: 2025-10-02.

[46] Linseis Messgeräte GmbH. Linseis-epoxy - thermal conductivity - technical datasheet. https://www.linseis.com/es/aplicaciones/polimeros/thb-100-epoxi-conductividad-termica/, 2025. Accessed: 2025-10-02.

[47] E. Solórzano, M.A. Rodriguez-Perez, and J.A. deSaja. Thermal conductivity of cellular metals measured by the transient plane sour method. *Advanced Engineering Materials*, 10(4):371–377, April 2008.

[48] Pablo Olivares and Jorge Manríquez. Análisis comparativo de la difusividad efectiva, artificial y real en materiales porosos. 2021.

[49] Alejandro Ramírez, John Jairo Castañeda, and Elizabeth Pabón. Estudio de las relaciones entre parámetros estructurales de sistemas porosos desordenados y la difusividad efectiva mediante monte carlo cinético. *Revista Facultad de Ingeniería Universidad de Antioquia*, (60):42–50, 2011.

[50] Hongyu Chen, Valeriy V. Ginzburg, Jian Yang, Yunfeng Yang, Wei Liu, Yan Huang, Libo Du, and Bin Chen. Thermal conductivity of polymer-based composites: Fundamentals and applications. *Progress in Polymer Science*, 59:41–85, August 2016.

[51] Tang Luping. A study of the quantitative relationship between strength and pore-size distribution of porous materials. *Cement and Concrete Research*, 16(1):87–96, January 1986.

[52] R. C. Progelhof, J. L. Throne, and R. R. Ruetsch. Methods for predicting the thermal conductivity of composite systems: A review. *Polymer Engineering amp; Science*, 16(9):615–625, September 1976.

[53] Giuseppe Pezzotti, Ikuko Kamada, and Sadao Miki. Thermal conductivity of aln/polystyrene interpenetrating networks. *Journal of the European Ceramic Society*, 20(8):1197–1203, July 2000.

[54] Warren M Rohsenow, James P Hartnett, Young I Cho, et al. *Handbook of heat transfer*, volume 3. Mcgraw-hill New York, 1998.

[55] James K. Carson. Modelling thermal diffusivity of heterogeneous materials based on thermal diffusivities of components with implications for thermal diffusivity and thermal conductivity measurement. *International Journal of Thermophysics*, 43(7), May 2022.